Near-Wall Flow Measurements Using Frequency-Modulating Filtered Rayleigh Scattering (FM-FRS)

Gwibo Byun[1]*, K. Todd Lowe[1], Michael Ellery[2], Joshua Sole[2]
1: Kevin T. Crofton Department of Aerospace and Ocean Engineering, Virginia Tech, USA
2: Prime Photonics LC, USA
* Correspondent author: gbyun@vt.edu

Keywords: Filtered Rayleigh Scattering, Frequency modulation, Near-the-wall velocimetry

Abstract

The frequency-modulating filtered Rayleigh scattering (FM-FRS) technique has been developed and applied for the boundary layer measurements. The FM-FRS technique effectively extracts Rayleigh scattering information from noisy low SNR signals caused by intense wall glare. The boundary layer velocity profiles measured by FM-FRS show excellent agreement with an independent pressure probe measurement and the law-of-the wall, including approximately 100 μm above the wall. This technique is desirable for the practical applications of the Rayleigh scattering technique for flow diagnostics to regions that were limited due to strong background and low signal-to-noise ratio.

1. Introduction

Accurately measuring boundary layer velocity profiles on test models is critical for understanding fundamental flow behaviors and associated complex phenomena near the model surface. It is also required for CFD model validations and further development, one of the significant test campaigns at large-scale wind tunnel facilities. Since some large-scale closed-circuit flow facilities do not permit the addition of seeded particles due to potential facility contamination, sensor damage, and safety concerns, the applications of seeded particle-based laser diagnostics are very limited to these circumstances. Therefore, non-intrusive seedless measurements are desirable and required for optical diagnostics to overcome those issues caused by seeding particles into the fluid. One of them is Rayleigh scattering measurement, which has matured much with the development of light sources and detectors. It is the interaction of light and matter on the scale of, or smaller than, the wavelength of the laser light. The probability of scattering increases with the number of molecules per volume, and molecules undergoing bulk motion in a flow impart a strong directional Doppler frequency shift. As described by the kinetic theory of gases, even stagnant gas molecules constantly move and impart a weaker, yet still measurable, Doppler shift that correlates to temperature. These are the key features of Rayleigh scattering signals that measure density and temperature, while the mean Doppler-shifted signal yields flow velocity. Therefore, Rayleigh scattering is very attractive due to its ability to determine Doppler-based velocity where seeding particles is not possible or undesirable. In addition to flow velocity, these key features make Rayleigh

scattering-based diagnostics ideal for in situ multi-property measurements. During the last decade, the frequency scanning filtered Rayleigh scattering (FS-FRS) technique has been developed and utilized for seedless velocimetry and scalar measurements for much more practical flow fields of scientific and engineering interest (Doll et al., 2017; 2018; Saltzman et al., 2019; Boyda et al., 2019, 2020a; Powers et al., 2022).

However, we have to overcome other scattering issues from the surface and particles for successful Rayleigh scattering measurements, which contaminate FRS signals and cause bias in the results. Residual particles in the facility flow stream will generate Mie scattering. The glare on the model surface will produce high-intensity background noise, making near-wall flow measurements more challenging than bulk flow measurements. Although one method of background mitigation we used effectively for planar measurements is structured light illumination (Boyda et al., 2020b), it is hard to keep the Rayleigh scattering signals near the wall region after filtering out the wall glare. Therefore, the near-wall boundary layer measurement will leverage an optical frequency modulation (FM) technique. The FM-FRS is a well-known technique (Mach and Varghese, 1999) that has been adapted from wavelength modulation spectroscopy. The FM-FRS technique better detects the convolution spectrum containing the Rayleigh scattering information from very noisy signals. Instead of directly using detected signals, the measured spectra's 1st and 2nd harmonics can be utilized to obtain velocity and scalar properties (temperature and density). Since the convolution spectrum is carried with the modulation frequency, measuring its harmonic signals will delineate the Rayleigh signal from noise sources, such as glare on the wall or surface.

Furthermore, due to the convolution of iodine vapor cell transmission and the broadband Rayleigh scattering spectra, Mie scattering by residual particles in flow will be filtered out. In contrast, the light by Rayleigh scattering will be transmitted and acquired at the trough of a scanning frequency band. The glare on the wall will be significantly reduced by scanning through the trough region. Therefore, this FM technique's advantages are expected to be 1) effective background removal, 2) improved spectral feature detectability using harmonic signals of the modulation frequency, 3) improved measurement accuracy of velocity and scalar properties, and 4) feedback control of laser frequency to avoid any spectral shape changes due to laser frequency drift during the measurements. The FM-FRS technique has been developed and applied in the present paper, especially for the boundary layer velocity measurements.

2. Experimental Setup

A small jet (ID = 17.5mm) has been built to perform a measurement using the FMFRS technique, as shown in Figure 1. It has a 3-axis traverse, co-flow generator, air filter, honeycomb, and screen to generate a uniform jet exhaust of Mach number 0.37. Kiel probes measure total pressure and total temperature at the plenum and jet exhaust. The jet profile has been measured using a Kiel probe, and its Mach number profile along the centerline is presented in Figure 1.

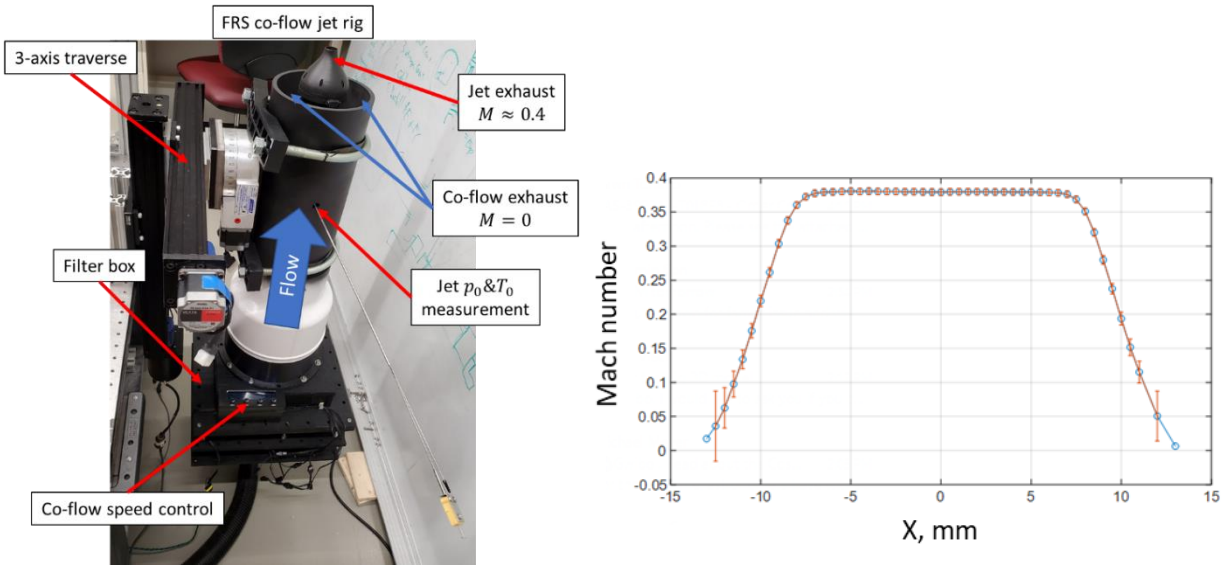

Figure. 1 Laboratory jet rig and Mach number profile of exhaust jet (30 mm above the nozzle).

The optical setup with the jet rig has been designed and integrated for the measurements. For the light source, a laser frequency scanning Verdi6 laser (Coherent, 532 nm) is leveraged with a function generator (Berkeley Nucleonics Corp, Model 645) and a high voltage amplifier (Trek, model 2205), which are required for Verdi laser piezo-electric (PZT) actuator to scan laser frequency. The laser is steered to cross the jet centerline and blocked by a beam dump. A total of three iodine vapor cells (12.7 cm long and 2 torr, Innovative Scientific Solutions Inc.) have been used to measure reference laser transmission and FRS spectra. The reference laser transmission is measured using amplified photodetectors (Thorlabs, PDA100A). A photomultiplier tube (Hamamatsu, H10721-01) is attached to the iodine cell to measure the convolved signals between the Rayleigh scattering spectrum and the iodine cell transmission spectrum. Those key components are presented in Figure 2. National Instrument (NI) PXIe system is used for data acquisition. The voltage outputs of PDAs and two PMTs are recorded by NI 9232 module. The total temperature at the plenum and jet exhaust are measured using a K-type thermocouple and recorded by NI 9213 module. A pressure scanner (Scanivalve, DSA3217) is used to measure total pressure at the plenum and jet exhaust.

As mentioned earlier, two PMTs are used to measure the convolved RS signal (FRS signal) at jet exhaust (PMT1) and no-flow (PMT2), as presented in Figure 3. The measurement of the no-flow FRS signal allows us to directly compare with the measured spectrum at jet exhaust for velocity determinations instead of generating a no-flow convolved spectrum using modeled Rayleigh scattering spectrum (Tenti et al., 1974; Pan et al., 2004) and iodine transmission spectrum (Forkey et al, 1997). The difference in temperature at the two measurement locations can affect the RS spectrum. However, the static temperature at two places would be less than 3 %, and its effect is negligible for the velocity determinations using the frequency modulating technique. Lock-in amplifiers (Stanford Research SR810 and SR830) are leveraged to measure

the amplitude of the 1st and 2nd harmonics of the low SNR signals directly to extract useful quantitative information from these FM-FRS signals from PMTs.

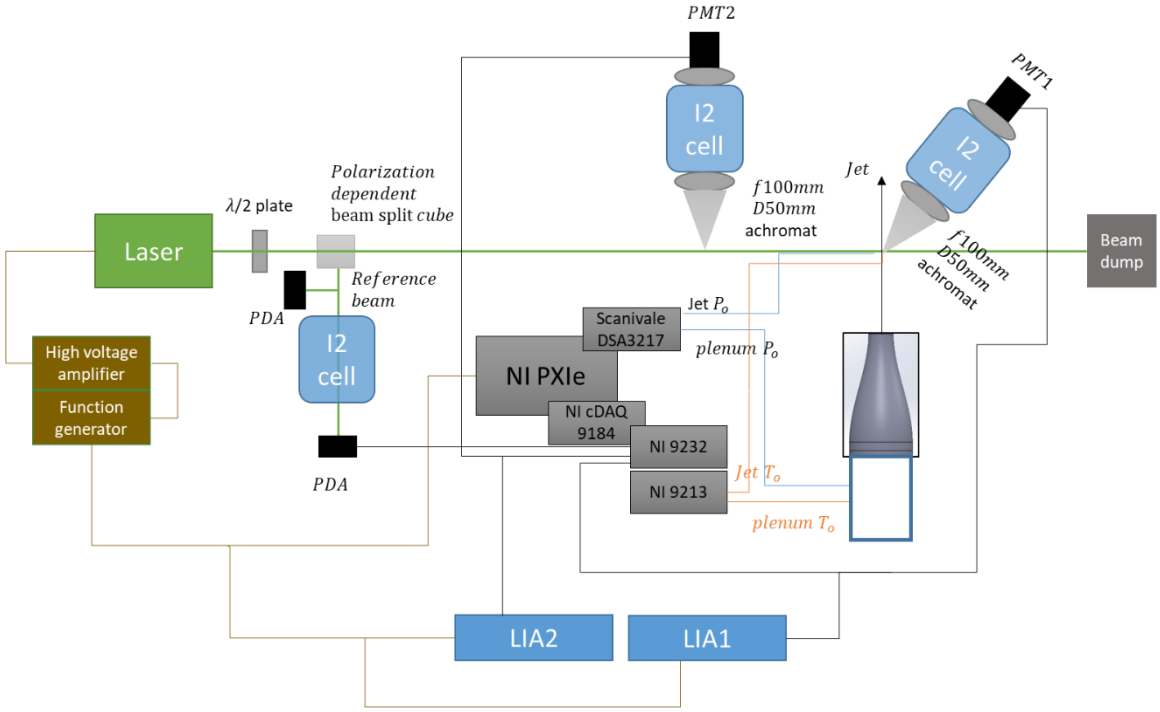

Figure. 2 FRS measurement setup (PMT: photomultiplier tube, LIA: Lock-in amplifier).

3. Results and Discussions

A. Free jet measurements

The designed and integrated measurement system has been validated by measuring a free jet velocity using the proposed FM-FRS technique and compared with the result of the Kiel probe measurement. Figure 4 shows the measured signals with the voltage output of the function generator. Note that the function generator output voltage is amplified by the high voltage amplifier (50 gain) and then supplied to a PZT actuator inside the Verdi laser head for laser frequency scanning. The reference transmission is leveraged to determine the scanned optical frequency range by comparing it with the modeled iodine transmission spectrum (Forkey et al., 1997). The FRS signal is measured at the jet exhaust, and Doppler-shift is observed caused by the jet compared with the reference transmission. Note that there are no ingested particles for the jet velocity measurements.

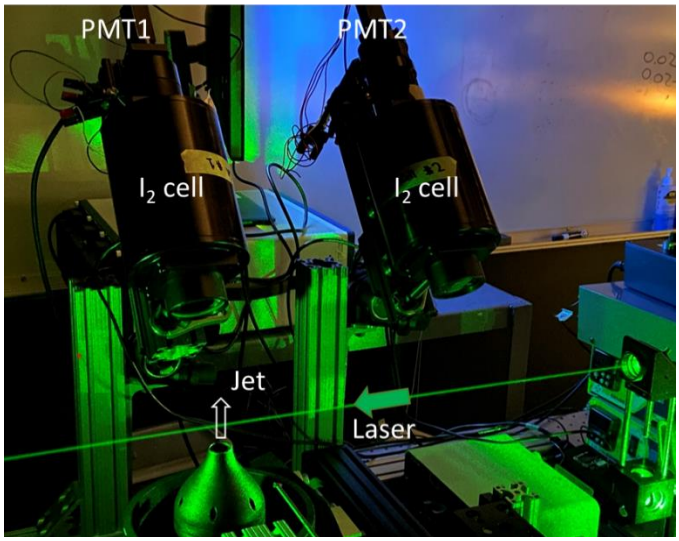

Figure. 3 Closed view of the measurement setup; PMT1 for jet detector and PMT2 for a no-flow detector.

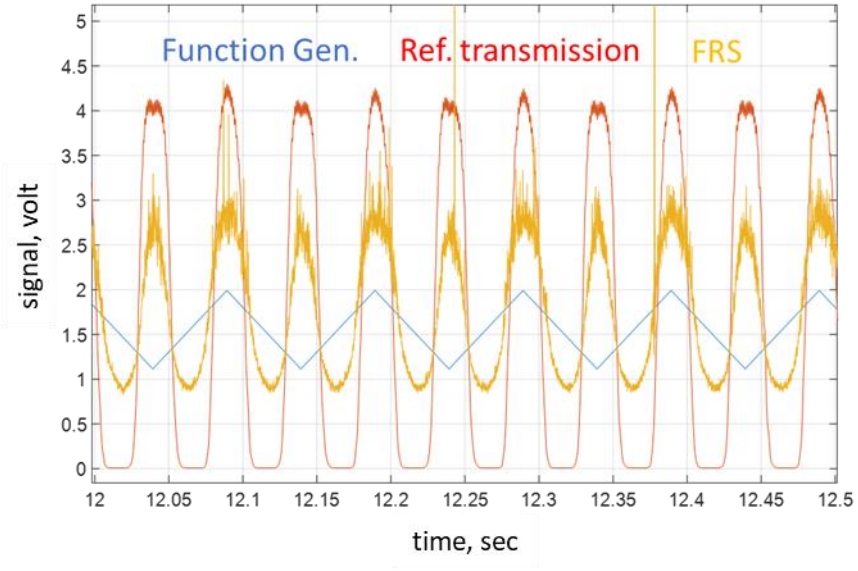

Figure. 4 Example of measured raw signals.

Since we use the iodine transmission spectrum of the reference beam to determine the wavenumber (laser frequency), we convert the scanning voltage to the wavenumber by fitting the measured transmission spectrum to the modeled transmission spectrum. Its result is presented in Figure 5. It shows that the iodine cell has a vapor pressure of 2 torr, which has a low transmission at a trough and is favorable to filtering out glare near the wall.

The laser was scanned for the jet velocity measurements between 18788.27 cm^{-1} and 18788.51 cm^{-1} as shown in Figure 5. A triangle wave was generated at 50 Hz and fed to the laser PZT actuator to scan the laser frequency. The signals of PDAs and PMTs were sampled at 50 kHz. The room temperature and pressure were 295 K and 13.7 psia, respectively. Figure 6 shows the

centered wavenumber vs. the measured signals of PDAs (I_2 cell transmission of reference beam), PMT1 (jet) and PMT2 (no-flow), respectively. The jet signal is noisier in the higher transmission region, which is caused by dust in the jet. As expected, the jet signal is shifted from the no-flow signal. Therefore, the mean velocity is calculated based on that shift obtained by least-square fitting for approximately 3,000 scanning cycles. The resulting mean velocity is 127 m/s, which shows a good agreement with the result of the Kiel probe measurement, 126 m/s. The FM-FRS technique was not required for the free jet measurements due to its high SNR. However, the near-wall region shows a much lower SNR, so the conventional least-square fitting is not applicable to achieve flow velocity.

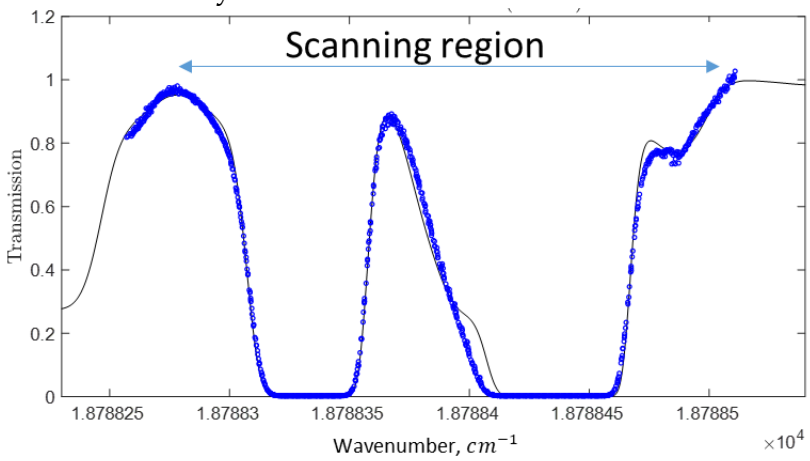

Figure. 5 Iodine cell transmission spectrum, measured (symbol), and theoretical model (solid line).

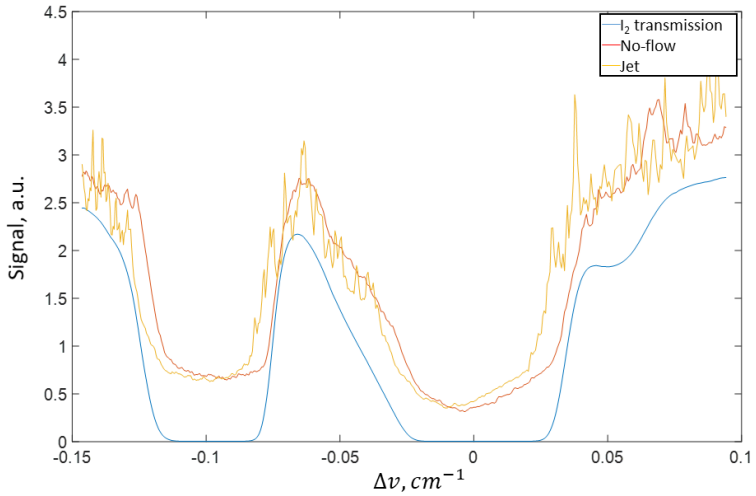

Figure. 6 Measured signal vs. wavenumber. Note the center wavenumber is 18788.4321 cm^{-1}.

Table. 1 Comparison of jet velocity measured by Kiel probe and FRS.

Kiel Probe	FRS
128 ± 1.2 m/s	129 ± 1.5* m/s

*RMS error of mean velocity from repeated measurements.

B. Near-wall flow measurement using FM-FRS

The jet was modified to measure boundary layer velocity profiles. Figure 7 presents a schematic and photo of the boundary layer measurement setup. A transparent acrylic plate (2mm thick) is attached to one side of the jet nozzle to generate the wall-bounded boundary layer flow and free-jet shear layer on the other side. It will produce wall glare near the plate caused by a laser beam, which is the main obstacle we need to resolve for successful near-wall measurements, as presented in the photo in Figure 7. For the comparison, an independent velocity measurement using a Kiel probe has been performed to validate the capability of the given FM-FRS technique for the near-wall boundary layer and free-jet shear layer measurements, especially mean velocities.

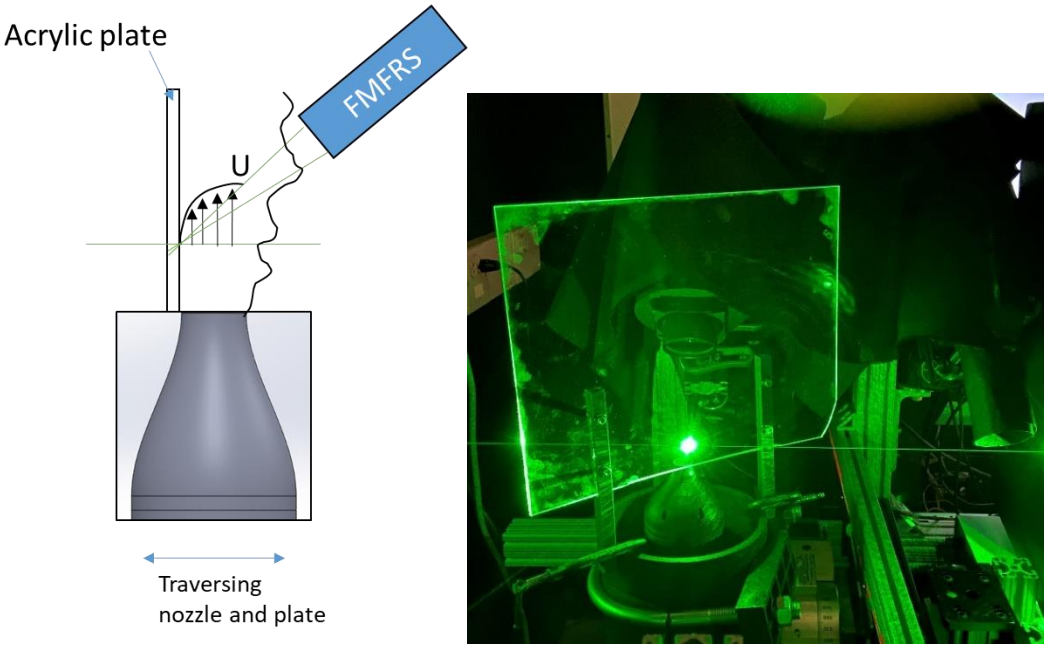

Figure. 7 Schematic of boundary layer measurements.
Note the measurement location is 20.6 mm downstream of the nozzle exit.

Figure 8 shows the laser glare on the plate and PMT signal at the near wall without jet flow. Note that the plate is 2 mm thick clear acrylic with an anti-reflection coating, and the beam power passing through the plate is 500 mW. The PMT signal is saturated except near the I_2 transmission trough region due to the glare on the plate. Several things affect the measurements with the wall glare: 1) laser power, 2) polarization, 3) PMT gain, 4) laser frequency scanning range, and 5) glazing angle. We no longer reduce the laser power, as a higher power is necessary for higher Rayleigh scattering at a given scanning frequency. Setting 500 mW is to simulate the achievable laser power out of fiber applications. The laser polarization needs to be set to minimize glare using a half-wavelength plate. The PMT gain can be reduced significantly to avoid signal saturation. However, the SNR of the detected signal will become very low at a

lower PMT gain. The scanning range of laser frequency needs to be set at the low transmission of an iodine cell to filter out the glaring light and detect Rayleigh scattering, which is another factor to lower the measured signal SNR. Figure 9 shows the measured signals without saturation. As expected, the SNR is much lower than the free jet (as presented in Figure 6) to process the conventional least-square fitting to measure the Doppler shift, causing a significant error. Therefore, more investigations have been performed to leverage the FM-FRS technique by measuring 1st and 2nd harmonics using a lock-in amplifier to overcome noisy low SNR signals at the near-wall region.

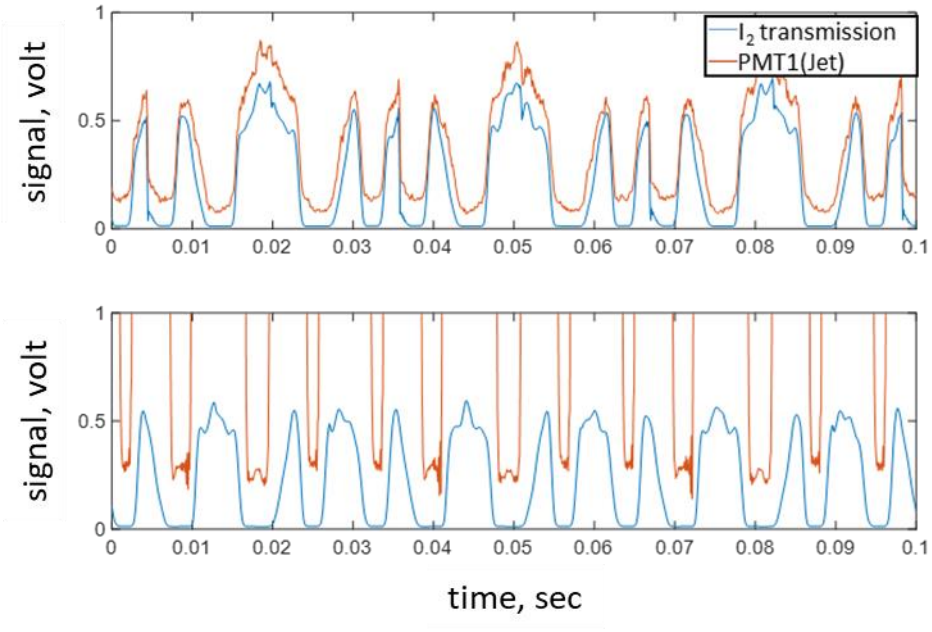

Figure. 8 PMT signal without (top) and with (bottom) the acrylic plate.

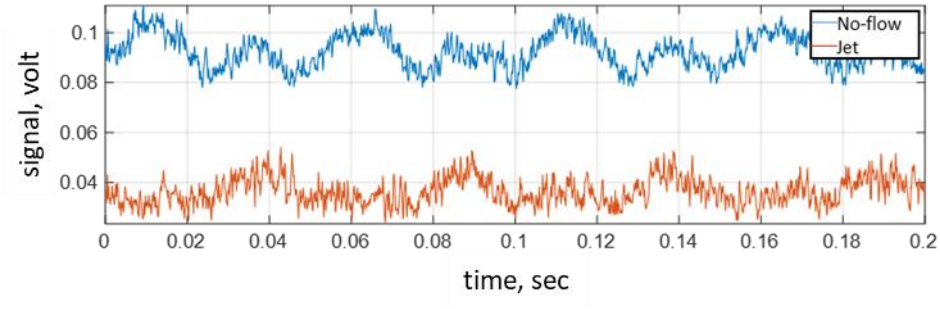

Figure. 9 PMT signals with the plate without saturation.

The principle of the FM-FRS technique is identical to FM Doppler global velocimetry (DGV) (Fisher et al., 2007; Fisher, 2017). Instead of using vapor cell transmission for FM-DGV, FM-FRS needs to use the convolution of vapor cell transmission and Rayleigh scattering spectrum as FM-FRS measures filtered Rayleigh scattering instead of Mie scattering. Therefore, this convolved

Rayleigh scattering spectrum can acquire the amplitude ratio of 1st and 2nd harmonics vs. wavenumber shift. Then, the Doppler shift caused by flow velocity is obtained by direct measurements of 1st and 2nd harmonics of detected signals. The 1st step is to set the center frequency and scanning range. The laser frequency range modulated for FM-FRS is presented, confirmed by the transmission measurement in Figure 10. The minimum transmission of the trough is approximately 10^{-6}, and the center frequency is 18789.9835 cm^{-1} for the presented results.

After defining the center frequency and scanning range, the amplitude ratio of 1st and 2nd harmonics is calculated for the shifted frequency. The model of the Rayleigh scattering spectrum (Tenti et al., 1974; Pan et al., 2004) has been used to obtain the convolved Rayleigh scattering signal with iodine transmission. Figure 11 shows the convolved Rayleigh scattering signal, an expected signal spectrum during the laser frequency modulation, and the simulated signals out of 6 sinusoidal cycles presented in Figure 12. These repeated signals are used to calculate 1st and 2nd harmonics and the ratio by using (Fisher, 2017)

$$\frac{A1}{A2} = \frac{\sum_{n=1}^{N} S(n)\cos\left[\frac{2\pi f_m}{f_s}(n-1)\right]}{\sum_{n=1}^{N} S(n)\cos\left[\frac{4\pi f_m}{f_s}(n-1)\right]} \qquad (1)$$

where A1 and A2 are the amplitude of 1st and 2nd harmonics, respectively, S is the simulated signal, f_m is the sinusoidal modulation frequency of 20 Hz, and f_s is the sampling frequency of 10 kHz. The A1/A2 vs. the shifted wavenumber is presented in Figure 13. Therefore, the shifted wavenumber and corresponding jet velocity can be obtained by direct measurements of A1 and A2 using Figure 13.

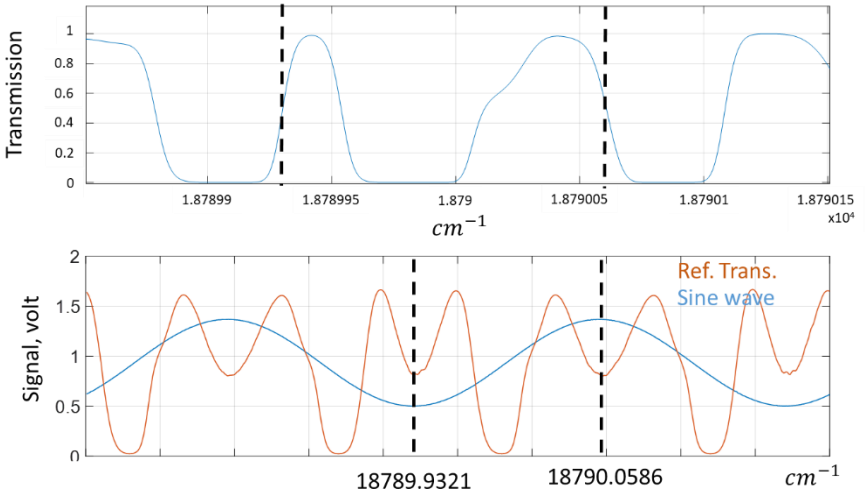

Figure. 10 Iodine cell (Reference beam) transmission; theory (Forkey et al., 1997) (top) and measured (bottom). Dashed lines denote the entire peak-to-peak scan range with 0.000146 cm^{-1}/mV. Note that the measured transmission (bottom) shows the repeated transmission by two sinusoidal modulation cycles.

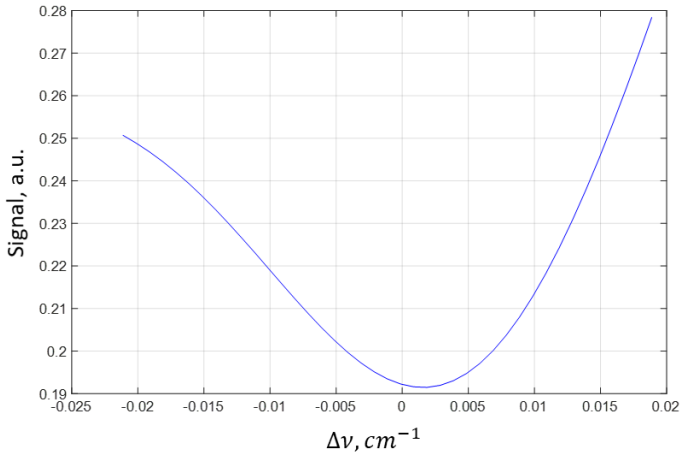

Figure. 11 Convolved Rayleigh spectrum of iodine transmission and Rayleigh spectrum of the scanning range of $\pm 0.02\ cm^{-1}$ from the center frequency, 18789.9835 cm^{-1}.

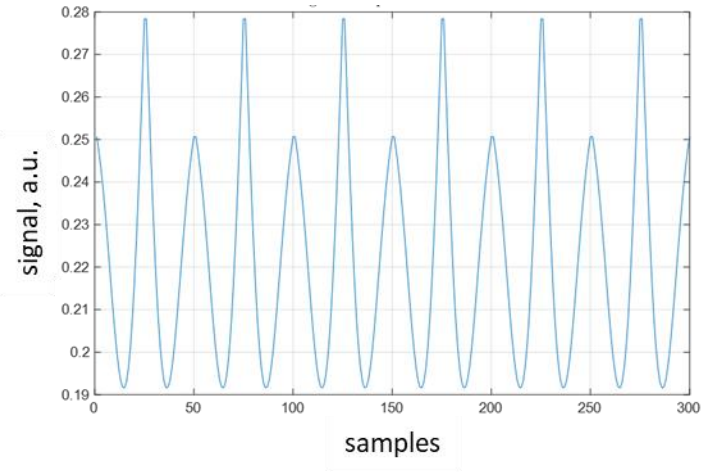

Figure. 12 Simulated FMFRS signal by sinusoidal modulation.

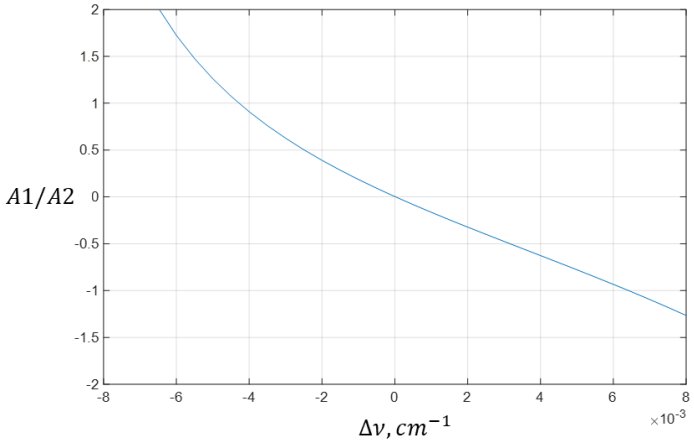

Figure. 13 The 1st and 2nd harmonic amplitude ratio vs. wavenumber shift.

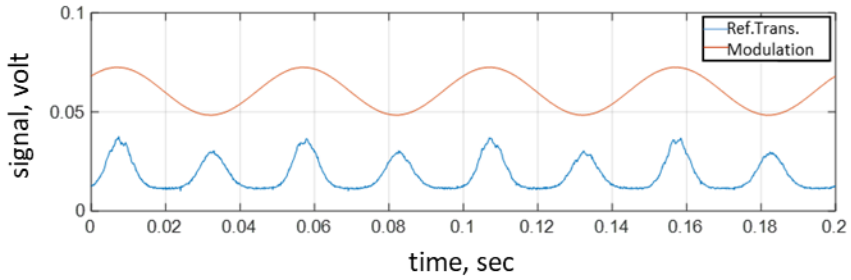

Figure. 14 Reference beam transmission vs. laser frequency modulating sine wave.

As mentioned earlier in Section B, a transparent acrylic plate is attached to the jet nozzle to generate the wall-bounded jet. Therefore, it is expected to measure the boundary layer, jet core, and jet shear layer across the current jet nozzle configuration. For FM-FRS, the laser frequency is modulated by a sinusoidal wave ($f_m = 20\ Hz$). Figure 14 shows the modulating wave and corresponding reference beam transmission. This reference beam transmission signal is being monitored for the scanning range of laser frequency for reference during the measurements. The sinusoidal wave offset has been adjusted to keep the scanning range consistent during the measurements.

One of the measured signals is presented in Figure 15. The signal is weak and noisy, and the glare is so intense that it contaminates the signal significantly at high transmission near the wall (top figure) compared with the signal away from the wall (bottom figure). As introduced earlier, the lock-in amplifiers (LIA) are leveraged to measure the amplitude of 1st and 2nd harmonics from these noisy and low SNR signals directly. Two LIAs are used, presented in Figure 16, one for no-flow PMT signals and the other for jet-flow PMT signals. Its time constant is set to 0.3 seconds to capture enough cycles for harmonic calculations. The laser frequency modulating sinusoidal wave is fed to LIAs to lock in at the modulation frequency (20 Hz). The amplitude and ratio of harmonics are saved and processed to calculate the shifted wavenumber and corresponding velocity. Note that the A1/A2 of no-flow signals provide essential information for laser frequency drifting despite monitoring the reference transmission and adjusting the offset of the sinusoidal wave. It gives the bound of laser frequency instability and choice for the A1/A2 of jet-flow signals within that bound (±1%) for post-processing. It could also be one of the most effective laser frequency PID control indicators, critical for the FM-FRS and any laser spectroscopic techniques. Note that the significant source of velocity uncertainty is caused by laser frequency drifting.

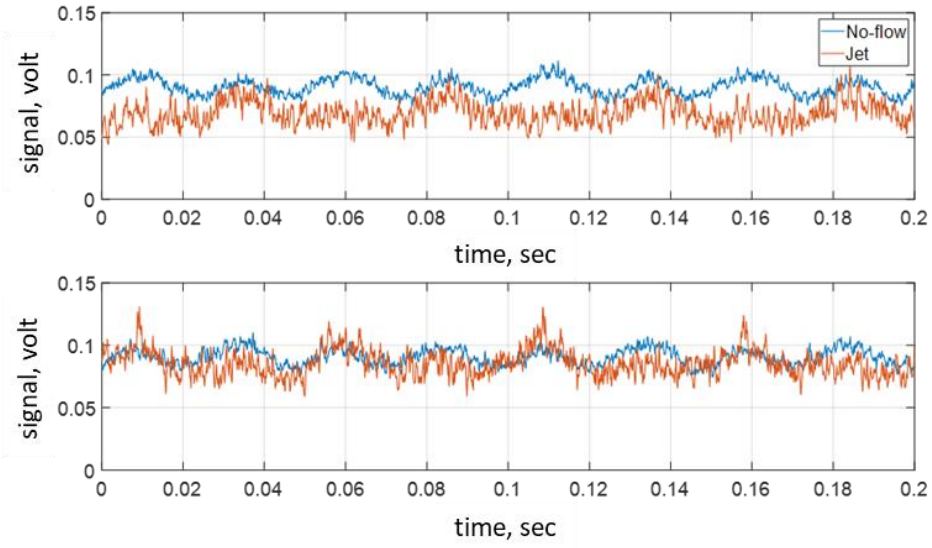

Figure. 15 Example of measured signals: Near the wall (1 mm, top) and away from the wall (10 mm, bottom).

The multiple jet velocity profiles across the jet nozzle are presented in Figures 17 and 18. The colored symbols represent FM-FRS results, while the black symbols represent the probe measurement results for comparison. First, the FM-FRS results agree with the probe results for the jet core and shear layer region within the uncertainty bounds. Note that the width of the jet core in Figure 17 is smaller than that in Figure 1, as it is measured along the off-center line. Second, the FM-FRS results for the wall-bounded boundary layer are presented in Figure 18. Directly comparing FM-FRS with the reference probe data is impossible as the probe data are unavailable below 1mm from the wall. Instead, the measured boundary layer profile is compared with the law of the wall (Spalding, 1961).

$$y^+ = u^+ + 0.1108\left[e^{0.4u^+} - 1 - 0.4u^+ - \frac{(0.4u^+)^2}{2!} - \frac{(0.4u^+)^3}{3!}\right] \quad (2)$$

Figure. 16 Lock-in amplifiers; Stanford Research SR810 (top) and SR830 (bottom)

where, $y^+ = yu_\tau/\nu$ and $u^+ = U/u_\tau$, and $u_\tau = \sqrt{\tau/\rho}$ is the skin friction velocity, which is estimated using the Schultz-Grunow formula (Schetz, 1993)

$$C_f = 0.0456(Re_\delta)^{-1/4} \tag{3}$$

For the law of the wall, the skin friction velocity, $u_\tau = 5.2$ m/s is used in equation (2). Compared with the law of the wall, the FMFRS technique can measure the log-layer as low as $y^+ \approx 30$ ($y \approx 100\ \mu m$ for the current jet conditions). Although the velocity uncertainty is high ($\pm$5 m/s) near the wall, it is a successful boundary layer measurement using the FRS technique without seeding particles up to the author's knowledge. Therefore, we are confident that the proposed FM FRS technique is promising for the seedless boundary layer measurements, including the near-wall region.

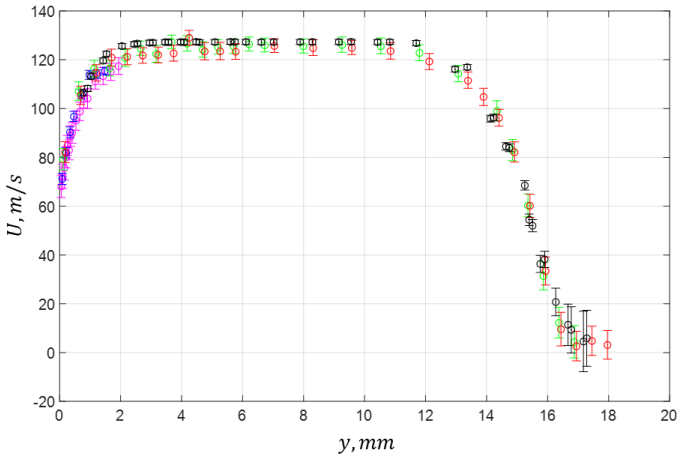

Figure. 17 The measured jet velocity profile.
Colored symbols: FMFRS, black symbols: pressure probe measurements.

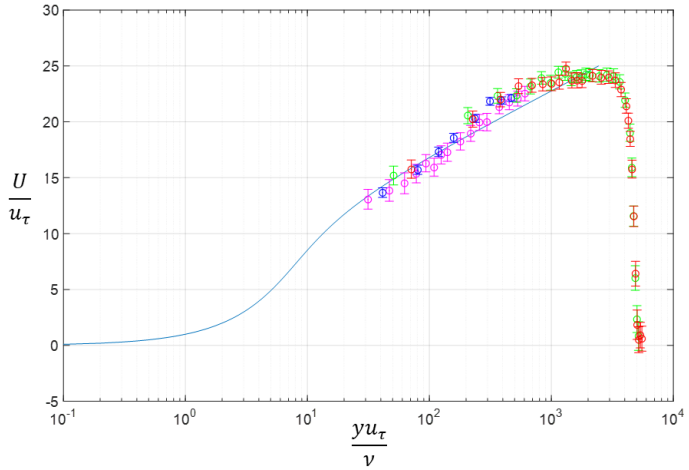

Figure. 18 The measured wall jet profile normalized by wall variables.
Solid lines: the law of the wall, symbols: FMFRS.

C. Velocity uncertainty

The velocity uncertainty of presented FM-FRS results is estimated to be up to ± 5 m/s. The primary uncertainty source during the measurements is laser frequency instability (wavelength jittering and drifting). Since the FM-FRS technique is based on the amplitude of 1st and 2nd harmonics, it is susceptible to the modulating range of laser frequency. The laser frequency is modulated by sinusoidal voltage input for the laser PZT actuator for the presented measurements. The drifting of the laser frequency range has been observed by monitoring the reference beam transmission, which results in the variation of the harmonic ratio, A1/A2, not caused by velocity fluctuations. Therefore, improving the laser frequency stability is critical to reducing the measurement uncertainty and increasing the accuracy of temporal measurements. A PID control by the feedback of no-flow A1/A2 would be one of the methods for improvement. Currently, it is estimated to be approximately 10 MHz wavelength instability. We can reduce the velocity uncertainty to 0.5 m/s if the laser frequency is controlled within sub-MHz.

The uncertainty of the probe data is estimated by using the specification of the pressure transducer, $\delta p = \pm 0.025\ psi$,

$$\frac{\delta U}{U_{max}} = \sqrt{\left(\frac{U}{U_{max}}\right)^2 + \frac{\delta p}{p_{max}}} - \frac{U}{U_{max}} \tag{4}$$

D. Cramér-Rao Lower Bound (CRLB)

The CRLB analysis, which yields velocity estimator variance, previously presented by Fischer et al. (2010), has been adapted for the current FM-FRS application. The signal model, $S(f) = QE\ n_s \tau(f)\ G$, is a function of the number of scattered photons (n_s), the quantum efficiency of the sensor (QE), the convolution of the iodine transmission spectrum and Rayleigh scattering spectrum, $\tau(f)$ as a function of laser frequency (f), and the gain (G). Two noise sources are considered for the CRLB: shot noise with Poisson distribution and electronic detector noise with Gaussian distribution. Therefore, the total $CRLB(U) = CRLB(U)_{Poisson} + CRLB(U)_{Gaussian}$ is acquired using Eqs (5) and (6).

$$CRLB(U)_{Poisson} = \frac{\sum_{k=0}^{N-1} \tau(f_k)}{\sum_{k=0}^{N-1} \frac{\tau'(f_k)^2}{\tau(f_k)} \sum_{k=0}^{N-1} \tau(f_k) - \left(\sum_{k=0}^{N-1} \tau'(f_k)\right)^2} \frac{\lambda^2}{2} \frac{1}{QE\ n_s} \tag{5}$$

$$CRLB(U)_{Gaussian} = \frac{\sum_{k=0}^{N-1} \tau(f_k)}{\left(\sum_{k=0}^{N-1} \tau(f_k)^2\right)\left(\sum_{k=0}^{N-1} \tau'(f_k)^2\right) - \left(\sum_{k=0}^{N-1} \tau(f_k)\tau'(f_k)\right)^2} \frac{\lambda^2}{2} \frac{NEP^2}{2{P_s}^2 T} \tag{6}$$

where, $\tau'(f)$ is $\frac{d\tau}{df}$, and N is the number of frequency scanning samples (100 samples were used for the current simulation), T is the duration of one velocity measurement (time constant of LIA), P_s is the light power of scattered photons, NEP and λ are the minimum noise equivalent

power of photodetectors and the laser wavelength, respectively. The NEP was estimated using the photodetector noise variance caused by dark current, σ_n^2

$$NEP^2 = \frac{\sigma_n^2}{\frac{f_a}{2}} \left(\frac{f_a hc}{QE\,\lambda}\right)^2 \tag{8}$$

where, f_a is the sampling frequency, h is the Planck constant, and c is the speed of light. The number of scattered photons (n_s) ranges $10^{2.3} \sim 10^4$ was considered for the signal simulations. Since the CRLB directly depends on $\tau(f)$, three different regions for the optical frequency scanning were selected, as shown in Figure 19. These three regions have been used for FRS measurements by authors. Note that region (c) was used for the presented FM-FRS experiments. The signal-to-noise ratio (SNR) is defined as $SNR = 10\log_{10}\frac{\sigma_S^2}{\sigma_P^2+\sigma_G^2}$, σ_S^2 is the variance of the noise-free signal, σ_P^2 is the signal-dependent Poisson-distributed shot noise, and σ_G^2 is the detector-dependent Gaussian-distributed noise, including constant random, dark, and readout noise. The simulated signals within the scanning wavenumber are presented in Figure 20 for the 4 dB ~ 29 dB SNR range.

The CRLB of the velocity estimator is shown in Figure 21. It is less than 1 m/s (0.8 % of jet core velocity) for all considered cases. Given the detector's specifications, the CRLB reduces with higher SNRs, which results from the increase in the number of detected photons (and P_s). Although there is no significant difference between the three regions, region (b) is recommended for the lowest CRLB. Also, filtering out the geometric scattering (wall glare) would be more efficient due to the lowest transmission in region (b).

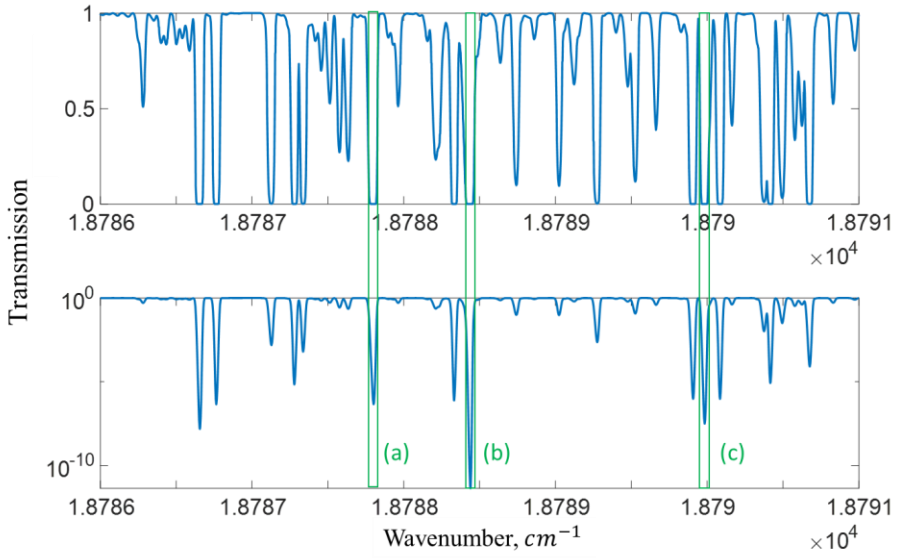

Figure. 19 Three regions of the iodine cell transmission spectrum for CRLB analysis. Linear scale (top) and log scale (bottom) of transmission.

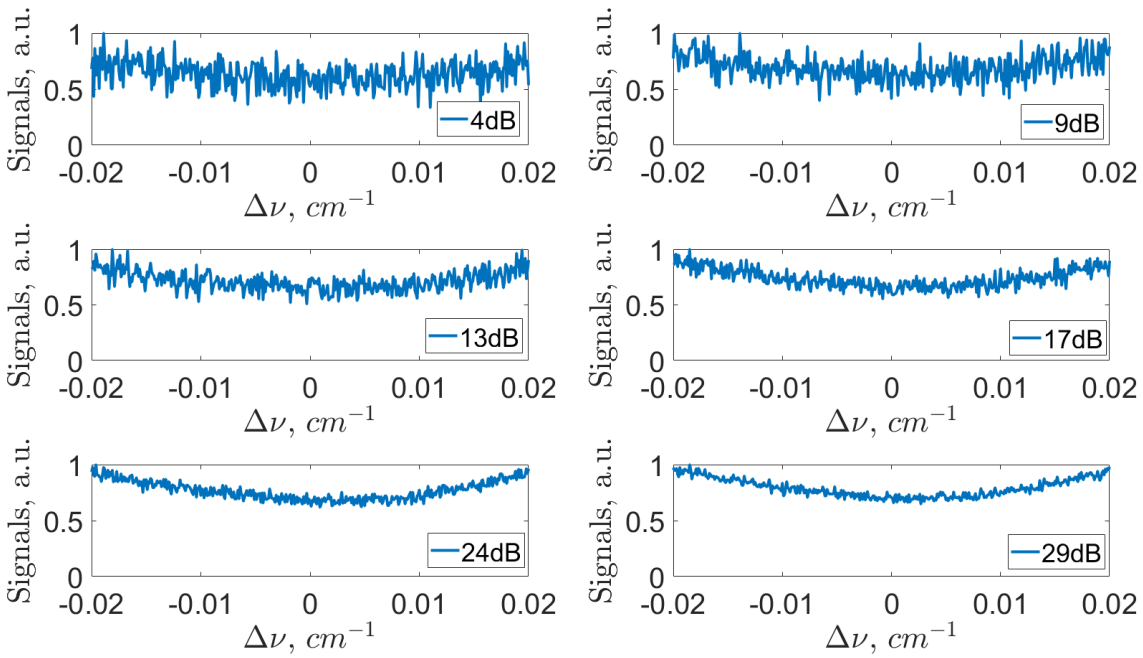

Figure. 20 The simulated signals for the region (a).

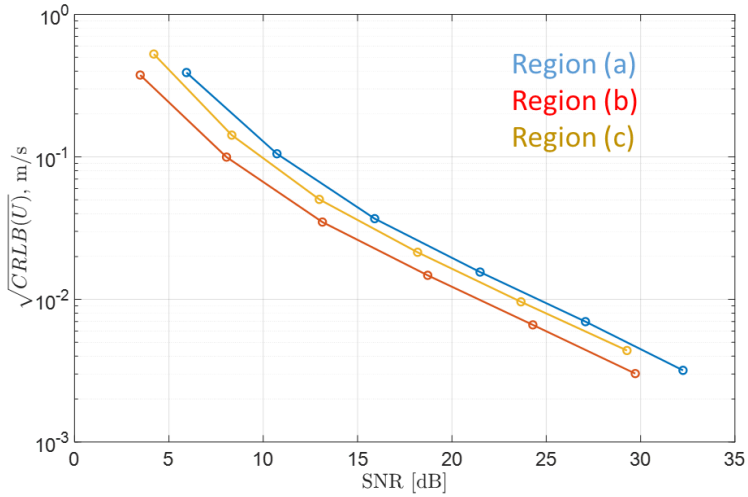

Figure. 21 The CRLB of velocity estimator vs. SNR for three scanning regions.

4. Conclusion

This paper describes the development and application of the FM-FRS technique to the measurements of boundary layer velocity profiles by detecting Rayleigh scattering, in which interest has been rising these days. As there is a common issue or limit to the applications of Rayleigh scattering to a wall-bounded or closed region of interest, the main challenge is to mitigate the glare on the wall and separate the Rayleigh scattering signals from the wall glare and background. The proposed FM-FRS method shows successful experimental results and validation of flow velocity measured within a boundary layer, a free jet, and a free shear layer. The successful implementation of PMTs and LIAs makes the presented FM-FRS technique

applicable for boundary layer measurement, including the near-wall region as close as approximately 100 μm to the wall within the measurement uncertainty of ±5 m/s. It would be the first application of FRS to resolve a log-layer and low SNR. The CRLB analysis for the velocity estimator using FM-FRS has been performed to investigate its lowest possible variance and the sensitivity of scanning ranges. It shows the feasibility of the FM-FRS technique for the near-wall region where the SNR is usually much lower due to the glare.

Further analysis is required to estimate the presented FM-FRS signal processing efficiency compared with the CRLB results. Based on the results and observations presented, the FM-FRS is a promising technique for seedless boundary layer measurements. Its hardware and software framework development can allow simultaneous velocity and scalar measurements with temporal and spatial resolutions.

Acknowledgments

This work was supported by NASA SBIR Phase I (Contract No. 80NSSC21C0389) with Paul M. Danehy as a technical monitor.

References

Boyda, M.T., Byun, G.B., and Lowe, K.T., (2019), Investigation of velocity and temperature measurement sensitivities in cross-correlation filtered Rayleigh scattering (CCFRS), *Meas. Sci. Technol.*, 30, 044004.
doi: 10.1088/1361-6501/ab0350

Boyda, M. T., Byun, G., Saltzman, A., Lowe, K. T., (2020a), Influence of Mie and geometric scattering on temperature and density measurements using filtered Rayleigh scattering, AIAA SciTech Forum 2020, Orlando, FL, AIAA-2020-1516.
doi: 10.2514/6.2020-1516

Boyda, M. T., Byun, G., Saltzman, A., Lowe, K. T., (2020b), Geometric scattering removal in cross-correlation Doppler global velocimetry by structured illumination, *Meas. Sci. Technol.*, 31, 064004.
doi: 10.1088/1361-6501/ab6b4f

Doll, U., Stockhausen, G., Willert, C., (2017), Pressure, temperature and three-component-velocity fields by filtered Rayleigh scattering velocimetry, *Optics Letters*, 42, 19, pp. 3773, 3776.
doi: 10.1364/OL.42.003773

Doll, U., Dues, M., Tommaso, B., Picchi, A., Stockhausen, G., Willert, C., (2018), Aero-thermal flow characterization downstream of an NVG cascade by five-hole probe and filtered Rayleigh scattering measurements, *Experiments in Fluids*. 59, 150.
doi: 10.1007/s00348-018-2607-z

Fischer, A., Büttner, L., Czarske, J., Eggert, M., Grosche, G., and Müller, H., (2007), Investigation of time-resolved single detector Doppler global velocimetry using sinusoidal laser frequency modulation, *Meas. Sci. Technol.*, 18, pp. 2529, 2545.
doi: 10.1088/0957-0233/18/8/029

Fischer, A., (2017), Model-based review of Doppler global velocimetry techniques with laser frequency modulation, *Optics and Lasers in Engineering*, 93, pp. 19, 35.
doi: 10.1016/j.optlaseng.2017.01.004

Fischer, A. and Czarske, J., (2010), Signal processing efficiency of Doppler global velocimetry with laser frequency modulation, Optik, 121, 20, pp.1891,1899.
doi: doi.org/10.1016/j.ijleo.2009.05.014

Forkey, J. N., Lempert, W. R., and Miles, R. B., (1997), Corrected and calibrated I2 absorption model at frequency-doubled Nd:YAG laser wavelengths, *Applied Optics,* 36:27: pp. 6729, 6738.
doi: 10.1364/AO.36.006729

Mach, J and Varghese, P.L., (1999), Velocity Measurements by Modulated Filtered Rayleigh Scattering Using Diode Lasers, *AIAA Journa*l, 37, 6, pp. 695, 699.
doi: 10.2514/2.797

Pan, X., Shneider, M. N., and Miles, R. B., (2004), Coherent Rayleigh-Brillouin scattering in molecular gases, *Phys. Rev. A.,* 69, 033814.
doi: 10.1103/PhysRevA.69.033814

Powers, S., Warner, E. P., Byun, G., Lowe, K. T., (2022), Auto-Processing of Filtered Rayleigh Scattering Images Including Mie and Background Scattering Contributions, 20th International Symposium on Application of Laser and Imaging Techniques to Fluid Mechanics, LISBON, PORTUGAL.

Saltzman, A., Boyda, M., Lowe, K.T., Ng, W.F., (2019), Filtered Rayleigh Scattering for Velocity and Temperature Measurements of a Heated Supersonic Jet with Thermal Non-Uniformity, 25th AIAA/CEAS Aeroacoustics Conference, Delft, The Netherlands, AIAA-2019-2677.
doi: 10.2514/6.2019-2677

Schetz, J.A, (1993), *Boundary layer analysis*, Prentice Hall, New Jersey, pp. 201, 214.

Spalding, D. B., (1961), A Single formula for the Law of Wall, *Journal of Applied Mechanics*, 28, 3, pp. 455, 458.
doi: doi.org/10.1115/1.3641728

Tenti, G, Boley, C. D., and Desai, R. C., (1974), On the kinetic model description of Rayleigh–Brillouin scattering from molecular gases, *Can. J. Phys.*, 52, pp. 285, 290.
doi: 10.1139/p74-041